

A novel approach to the use of earth observation to estimate daily evaporation in a sugarcane plantation in Xinavane, Mozambique

den Besten, N. I.; Kassing, R. C.; Muchanga, E.; Earnshaw, C.; de Jeu, R. A.M.; Karimi, P.; van der Zaag, P.

DOI

[10.1016/j.pce.2020.102940](https://doi.org/10.1016/j.pce.2020.102940)

Publication date

2021

Document Version

Final published version

Published in

Physics and Chemistry of the Earth

Citation (APA)

den Besten, N. I., Kassing, R. C., Muchanga, E., Earnshaw, C., de Jeu, R. A. M., Karimi, P., & van der Zaag, P. (2021). A novel approach to the use of earth observation to estimate daily evaporation in a sugarcane plantation in Xinavane, Mozambique. *Physics and Chemistry of the Earth*, 124(1), Article 102940. <https://doi.org/10.1016/j.pce.2020.102940>

Important note

To cite this publication, please use the final published version (if applicable). Please check the document version above.

Copyright

Other than for strictly personal use, it is not permitted to download, forward or distribute the text or part of it, without the consent of the author(s) and/or copyright holder(s), unless the work is under an open content license such as Creative Commons.

Takedown policy

Please contact us and provide details if you believe this document breaches copyrights. We will remove access to the work immediately and investigate your claim.



A novel approach to the use of earth observation to estimate daily evaporation in a sugarcane plantation in Xinavane, Mozambique

N.I. den Besten^{a,b,*}, R.C. Kassing^b, E. Muchanga^c, C. Earnshaw^c, R.A.M. de Jeu^a, P. Karimi^d, P. van der Zaag^{b,d}

^a VanderSat, Haarlem, The Netherlands

^b TU Delft, Delft, The Netherlands

^c Tongaat Hulett Xinavane, Xinavane, Mozambique

^d IHE Delft, Delft, The Netherlands

ARTICLE INFO

Keywords:

Remote sensing
Evaporation
Priestley–Taylor equation
Sentinel-2
Albedo
NDVI
Irrigation

ABSTRACT

Efficient irrigation water management for an 18,000 ha sugarcane plantation in Xinavane in southern Mozambique is a challenge. Sugarcane is an irrigation intensive crop and its productivity is sensitive to water stress. Options to adopt field water management best practices and proper irrigation scheduling are limited due to the lack of plot-level information on the actual crop water use and stress levels throughout the growing season. Due to heterogeneity in cropping calendar within the sugarcane plantation, at a certain point of time, different plots are at different growth stages. This makes scheme level irrigation scheduling complex and calls for frequent crop water use information. To fill this gap, this study presents a novel approach where a combination of satellite imagery with local weather data is used to provide daily evaporation rates. The Priestley–Taylor equation is applied to quantify evaporation (soil evaporation + transpiration) using radiation and temperature data from a meteorological station and spatial albedo estimates derived from the Sentinel-2 satellites. The results show 20 meter resolution maximum crop evaporation estimates can be derived with the proposed methodology. Additionally, the results show NDVI in the last two crop stages is able to distinguish between poor and good performing fields. Therefore, NDVI can be a useful index to estimate actual evaporation. First, the evaporation estimates were corrected for the crop stage using NDVI proxies and an additional stress indicator was used to calculate the actual evaporation flux spatially. The spatial evaporation estimates provide the water manager with information on actual crop water use and biomass development, which is relevant to both crop monitoring and irrigation management water management when drought-related stress is filtered.

1. Introduction

Globally agriculture accounts for approximately seventy percent of the total fresh water withdrawals (FAO, 2016b). To cope with the increasing competing demands for water in river basins it is necessary to focus on enhancing water use efficiency and water productivity in irrigated agriculture which is the largest water consumer sector. Due to its importance and urgency this goal is referred to in the UN sustainable development goals (SDGs) under the target 6.4 which calls for substantial increase in water-use efficiency to address water scarcity.

The predominant irrigation technique, globally, is surface irrigation which accounts for 86% of the total (FAO, 2016b; Berg and Carter, 1980). Surface irrigation is considered an irrigation method with a low water use efficiency. Poor field water management practices in surface

irrigation often result in drainage issues and erosion (Berg and Carter, 1980), salinization (Aroca, 2012), and low field irrigation application uniformity (Raine and Bakker, 1996). These issues all lead to reducing gains, and low land and water productivity (Gunarathna et al., 2018; Singh et al., 2018).

Sugarcane, with a global cultivated area of 26 million hectares, is widely used as an industrial crop to produce bioethanol and sugar (Endres et al., 2018). The economic contribution of this commercial crop is of vital importance to some of the African economies such as Mozambique (Jelsma et al., 2010). As a water-intensive crop, sugarcane often requires frequent irrigation (Endres et al., 2018). Its large scale cultivation is known to highly impact freshwater abstraction rates (Olivier and Singels, 2015). The majority of the irrigated sugarcane is irrigated

* Corresponding author at: VanderSat, Haarlem, The Netherlands.
E-mail address: ndenbesten@vandersat.com (N.I. den Besten).

using surface irrigation method (FAO, 2016a) and its productivity is prone to inherent challenges that surface irrigation has.

Proper water management is essential in achieving the target crop yield for sugarcane. The yield is sensitive to both water stress and waterlogging, a situation in which the soil remains saturated with water for prolonged periods. In water stress conditions the plant closes stomata pores to avoid water losses, leading to a decrease in transpiration and subsequently reduced biomass production (Aroca, 2012). Short periods of water logging mostly do not result in a sugarcane yield decrease, nor decrease in transpiration, but it is observed that if flooding is persistent (>21 days) or if the water tables are very shallow (<15 cm) biomass growth can be significantly hampered (Chabot et al., 2002; Glaz et al., 2004). In addition, the salinity of the soil and/or irrigation water decreases the stomatal conductance and photosynthesis and inhibits the growth of sugarcane (Plaut et al., 2000).

Water stress may lead to curling of sugarcane leaves, alteration in chlorophyll content of the plants, reduced leaf area, and stomatal closure (Ferreira et al., 2017; Inman-Bamber and Smith, 2005). These symptoms of stress can be observed by the over-passing satellites, which observe vegetation status of the growing crops, and surface temperature, amongst other variables. This data can be used to derive spatial evaporation estimates. These spatial evaporation estimates can be very helpful in efficiently allocating water in especially irrigated agriculture (Bastiaanssen et al., 2000).

Several algorithms have been suggested to retrieve evaporation estimates from data collected by orbiting satellites. For instance, the Two Source Energy Balance (TSEB) (Norman et al., 1995), the Surface Energy Balance Algorithm for Land (SEBAL) (Bastiaanssen et al., 1998), the Atmosphere–Land Exchange Inverse (ALEXI) model (Anderson et al., 2007), and the Global Land-Surface Evaporation: the Amsterdam Methodology (GLEAM) (Miralles et al., 2011), and the FAO Water Productivity Open-access portal (FAO). These algorithms apply different methodologies to derive crop water stress and estimate actual evaporation. For example, within GLEAM stress is integrated as a function of the availability of water in the root-zone and canopy size, using microwave soil moisture observations and vegetation optical depth (Miralles et al., 2011). With the Alexi and TSEB models information from the thermal band is used to detect crops stress, based on the principle that canopy temperature increases with increasing crop stress (Anderson et al., 2007).

To serve the needs of agricultural management at field level and within a field, a high spatial and temporal resolution is required. With the launch of the Copernicus Sentinel-2 satellites, valuable high spatial resolution imagery became available which can assist field-scale and within field agricultural management (Vanino et al., 2018).

Several authors have demonstrated or researched the use of spatial evaporation estimates based on satellite remote sensing to estimate and visualize the crop water requirement to assist irrigation planning (Vuolo et al., 2015; Vanino et al., 2018, 2015; FAO; Atzberger, 2013; Mulla, 2013; Bastiaanssen et al., 2000). Detailed evaporation estimates can be used in (irrigation) water management to estimate the crop water requirement or maximum crop evaporation. For instance, this information can be used to irrigate at the proper time and with the proper amount per field. Optimizing irrigation water use, in an irrigation scheme, can benefit from frequent spatial evaporation updates on the actual development of the crop and its water requirement (Vuolo et al., 2015; Vanino et al., 2018; Calera et al., 2017). This is because farmers tend to over irrigate in the absence of objective information on crop status and water requirement (Vanino et al., 2018).

An operational irrigation monitoring system that incorporates near real-time high spatial resolution evaporation information in irrigation decisions and practices will be a significant improvement over the point-based evaporation estimates which are still common even within relatively hi-tech plantations and irrigation schemes (Inman-Bamber and McGlinchey, 2003; Singels et al., 1998). High spatial resolution evaporation estimates enable plantations to monitor water needs at and

within the plots, keep track of crop growth, take corrective actions when necessary, and consequently leading to better yields (Calera et al., 2017).

Previous studies demonstrating high spatial resolution evaporation estimates have combined meteorological and satellite data (Vuolo et al., 2015; Vanino et al., 2018, 2015). Information on Leaf Area Index (LAI) and albedo was retrieved by Sentinel-2 imagery, whereas other data was obtained from a nearby meteorological tower (Vanino et al., 2018). These methodologies use the FAO-56 Penman Monteith method as a basis for their calculations to estimate maximum crop evaporation and irrigation water requirements (Allen et al., 1998).

In this research we focus on a sugarcane plantation in Xinavane in southern Mozambique. The Priestley–Taylor methodology is used to get spatial evaporation estimates (Priestley and Taylor, 1972). Due to the mono-culture in the plantation we are able to develop a sugarcane specific remote sensing evaporation estimate. The application of the Priestley–Taylor (PT) methodology with satellite data has so far shown promising results in several remote sensing based evaporation algorithms and studies (Miralles et al., 2011; Fisher et al., 2015; Chen et al., 2014). However, these researches do not apply their research in an irrigated context. Priestley–Taylor requires limited data and parameterization and therefore fits the study due to the limited data availability (Fisher et al., 2015).

The objective of this study is to present a novel approach for estimating daily actual evaporation at a high resolution of 20 m using a combination of satellite imagery and local weather data. The analysis focuses on a furrow-irrigated area within the plantation, covering 420 hectares. This area was part of a pilot project IWACA-Tech, which aimed at improving water use efficiency at irrigation systems using advanced remote sensing technology.¹

2. Methodology and data

2.1. Study site

The Xinavane plantation is located within the lower reaches of the Incomati river basin, in Mozambique (Fig. 1). The irrigated sugarcane plantation in Xinavane is in competition over water with the increasing population and water users in upstream South Africa and Swaziland where numerous sugarcane plantations are located (Santillán-Fernández et al., 2016; Van der Zaag and Carmo Vaz, 2003). From 2012 until 2014, the plantation experienced three successive seasons of flooding which adversely affected the operations within the plantation. These events were followed by two consecutive drought years in 2015 and 2016, associated with El Nino (Gelcer et al., 2018). In the years 2017 and 2018 the annual rainfall was also below average.

Twenty-four furrow irrigated fields of the IWACA-Tech project were selected for the analysis, with a total area of approximately 420 ha (Fig. 1). The slope runs from Northwest to Southeast in the study area. The irrigation interval is approximately 10–12 days, and the net irrigation application depth aimed by the agricultural department is 1,350 mm/year. The long-term, 1967 to 2017, average annual precipitation in the area is 721 mm/year.

2.2. Sugarcane growth characteristics

The furrow irrigated study site plots have a size of approximately 20 ha each. Within the sugarcane plantation, sugarcane is harvested after approximately 12 months when the crop is nearly four meters tall. From April to December fields are harvested based on the production capacity of the factory, meaning the crop stages and length of growing season differ between fields.

¹ www.iwacatech.com.

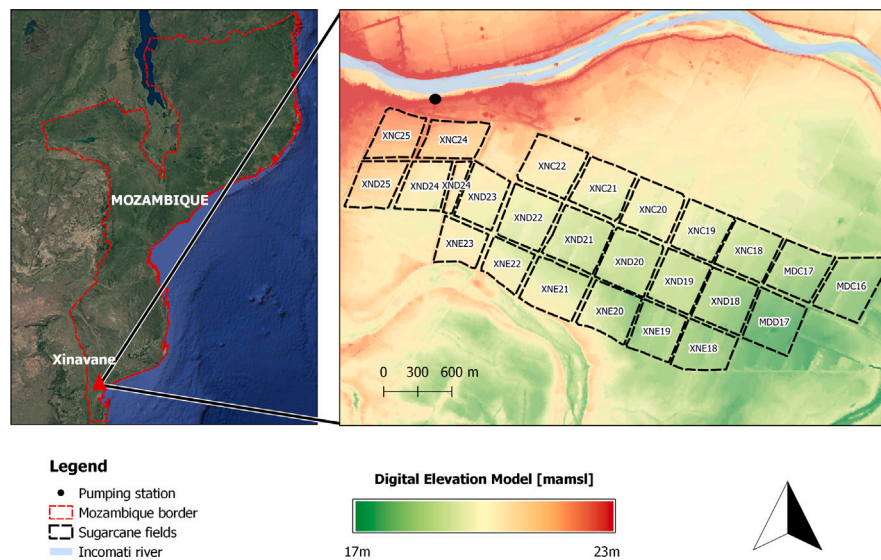


Fig. 1. The left panel shows the location of the sugarcane plantation in Xinavane, Mozambique. The map on the right zooms in to the project site.

Sugarcane is grown as a ratoon crop, so new cane grows from the same root in 8–9 consecutive years. Ratooning naturally leads to a decline in yield over the years, due to several factors, such as soil degradation and fertility (Yadav et al., 2009). Sugarcane growing stage is often divided into four periods: an initial stage (30 days), tillering stage (90 days), development stage (150 days), and the final stage (90 days) (Doorenbos and Pruitt, 1977; Silva et al., 2015). In these different stages the consumptive water use differs and, therefore, it is important to characterize the different stages for agricultural water management. The initial stage commences right after harvest or planting, characteristic for this stage is the germination of the original stool. After the initial stage, the tillering stage commences, during which the sprouted sugarcane rapidly starts to form shoots and leaves. Next, the smaller shoots die off due to plant competition, and the elongation of the stem starts in the development stage. In this stage, not many new leaves are formed, but energy is used for the growth of existing leaves and the stalk (Cock, 2001). The final stage of the sugarcane crop is characterized by senescence, where the plant cells degrade and the end of the crop cycle approaches (Martins et al., 2016).

2.3. Field data

Data for this research was shared by the agricultural department of Xinavane's estate. This included data on planting dates, harvesting dates, and yields in the period between April 2012 and June 2018. The critical level for yield in the sugarcane plantation is defined as 80 tonnes sugarcane per hectare (tonnes/ha) by the estate management. Fields below the critical level will trigger a diagnostic performance assessment by the plantation management and will be followed up by corrective measures. The set target yield is 105 tonnes cane per hectare.

We also studied the spatial differences in yield during the growing seasons of 2016–2017 and 2017–2018. To compare different fields adequately, fields were selected with the same growing period for an in-depth analysis, since the yield is affected by the harvest date. The selected fields were clustered to good performing (>90 tonnes/ha), medium performing (80–90 tonnes/ha) and poor performing (<80 tonnes/ha) fields. Table 1 presents the selected fields and Fig. 1 shows the location of these particular fields. Table 1 displays the yield of the fields in the year of the analysis, the planting date, and the harvest date with the nearest Sentinel-2 overpass date used as a final date for the analysis.

2.4. Reference evaporation

The full workflow proposed in this paper is visualized in Fig. 2. In order to take the first step in estimating the actual evaporation spatially with the available data, we first estimated the reference evaporation with Priestley–Taylor (Priestley and Taylor, 1972). The methodology and input used to get the reference evaporation are visualized in the first column of Fig. 2. Priestley–Taylor describe the evaporation from saturated surfaces into an unsaturated atmosphere, which is expressed as a function of an equilibrium rate (Viswanadham et al., 1991). According to Priestley–Taylor, the daily evaporation rate can be defined as:

$$E_{PT} = \frac{1}{\gamma} \cdot \frac{s(R_n - G)}{s + \lambda} \cdot \alpha \quad (1)$$

where E_{PT} is the daily evaporation flux (mm d^{-1}), γ the latent heat of vaporization (2.45 MJ kg^{-1}), s the slope of saturation vapor pressure–temperature relationship (kPa C^{-1}), α is a dimensionless empirical number and better known as the Priestley–Taylor coefficient [-], R_n the net radiation ($\text{MJ m}^{-2} \text{ d}^{-1}$), λ the psychrometric constant (kPa C^{-1}), and G the soil heat flux ($\text{MJ m}^{-2} \text{ d}^{-1}$), which is assumed negligible when averaged over a day (Price, 1982).

The net radiation is computed by balancing the incoming shortwave radiation and incoming L_{in} and outgoing L_{out} longwave radiation. The latter is calculated through the surface and air temperatures in combination with the Stefan–Boltzmann law, to determine the temperature flux for sensible heat. Air temperature data was obtained from the estate's weather station.

Daily Land Surface Temperature and Emissivity (LST and E) at 1 kilometer (km) spatial resolution was derived from the MOD11A1 Version 6 product from the MODIS Terra satellite (Wan et al., 2015). The surface albedo, r_0 , controls the partitioning of incoming shortwave radiation R_g . R_g data was also obtained from the local weather station. The net radiation R_n can be calculated as:

$$R_n = (1 - r_0)R_g + L_{in} - L_{out} \quad (2)$$

Data on surface temperature from (MODIS), air temperature and incoming shortwave radiation data of the meteorological station were used in combination with spatially distributed albedo maps. Combining spatial satellite data with meteorological data requires combining data layers with different spatial and temporal resolutions. This has been successfully done by other authors, such as Vuolo et al. (2015) and Vanino et al. (2018). Combining resolutions is possible because not

Table 1

An overview of three groups of fields that were considered for analysis with a similar harvest date and length of growing season. The rows indicate the yield (tonne/ha), planting date, harvest date with the date of the nearest Sentinel overpass.

Group 1					
	XNC18 (ratoon 5)	XNE22 (ratoon 4)	XND19 (ratoon 8)	MDD17 (ratoon 7)	XND24 (ratoon 8)
Yield 2017 (tonne/ha)	110.3	93.5	92.5	44.0	50.4
Planting date	5/28/2016	7/26/2016	7/22/2016	6/18/2016	5/28/2016
Harvest date (Overpass)	6/3/2017 (5/19/2017)	6/25/2017 (6/28/2017)	7/10/2017 (6/28/2017)	7/12/2017 (6/28/2017)	6/15/2017 (11/22/2017)
Group 2					
	MDC17 (ratoon 7)	MDC16 (ratoon 7)	XNE19 (ratoon 4)	XNC19 (ratoon 6)	XNC22 (ratoon 5)
Yield 2017 (tonne/ha)	68.8	53.3	86	90.4	71.9
Planting date	11/14/2016	11/16/2016	11/26/2016	11/11/2016	12/8/2016
Harvest date (Overpass)	12/21/2017 (11/22/2017)	12/17/2017 (11/22/2017)	12/17/2017 (11/22/2017)	12/17/2017 (11/22/2017)	12/19/2017 (11/22/2017)
Group 3					
	XNC18 (ratoon 6)	XNE22 (ratoon 5)	XND18 (ratoon 8)	XND20 (ratoon 9)	
Yield 2018 (tonne/ha)	89.3	90.7	66.8	69.7	
Planting date	6/3/2017	6/25/2017	6/16/2017	7/10/2017	
Harvest date (Overpass)	6/4/2018 (5/11/2018)	5/26/2018 (5/11/2018)	5/31/2018 (5/11/2018)	6/21/2018 (6/10/2018)	

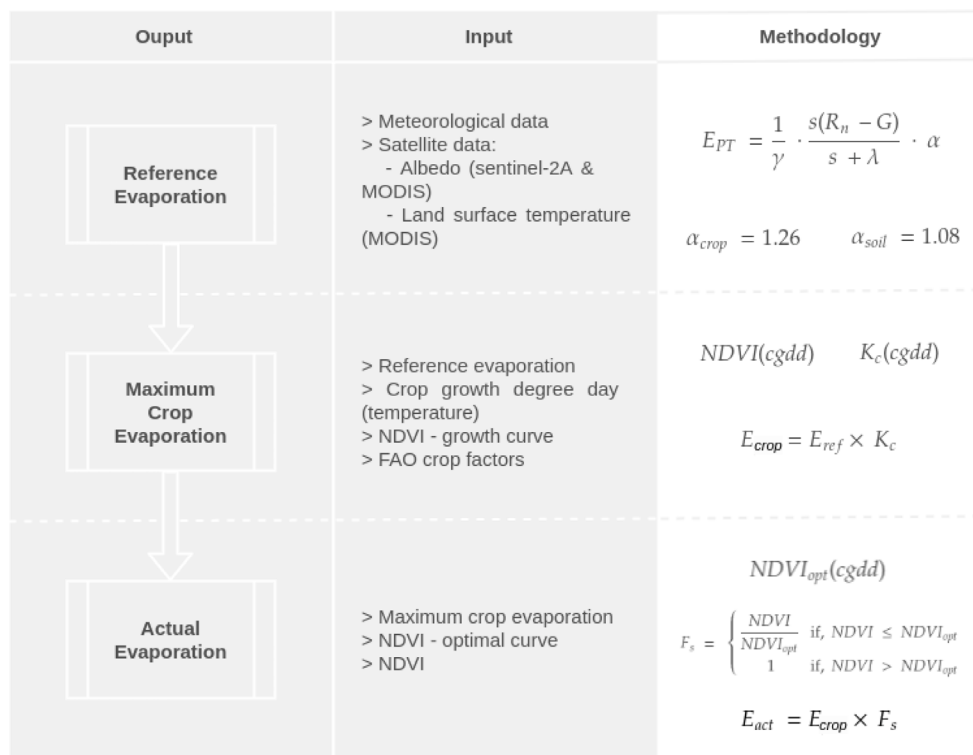


Fig. 2. A visualization of the methodology.

all variables show large variability spatially (e.g. incoming radiation) or temporally (e.g. albedo). To illustrate, incoming shortwave radiation can be covered by daily meteorological point measurement, because there is little spatial variability. In contrast, albedo varies spatially, but shows less variability temporally, and therefore can be estimated with the help of satellite data.

The albedo is calculated using two spectral signature curves: one for sugarcane (Apan et al., 2004) and one for clay soil (Vertisol, obtained from Aster Spectral Library (Meerdink et al., 2018)). The signatures were used to extrapolate the reflection registered within the different bands of Sentinel 2. To continue, the reflection within the same bandwidths as the satellite observations in the spectral signature curves were

averaged ($\rho_{b,rc}$) for the respective Sentinel-2 bands. The reflectance observed in the sentinel bands ($\rho_{b,s}$) were divided by $\rho_{b,rc}$, weighted according to the band contribution to the total w_b , and summed to get a correction factor (C_f) to reconstruct the reflection curve for each pixel:

$$C_f = \sum ((\rho_{b,s}/\rho_{b,rc}) \times w_b) \quad (3)$$

Finally, the albedo was estimated over the extent of spectral reflection curves. Additionally, the computed albedo was scaled with the BRDF/albedo Parameters Daily L3 Global Version 6 of MODIS to correct for overestimation caused by limited observation bands of Sentinel-2 (Schaaf and Wang, 2015). Sentinel-2 data is available at a 5-day interval. For the construction of the albedo daily time series, only Level 2A (Louis et al., 2016) and cloud-free images were used. Missing dates were linearly interpolated. This resulted in daily albedo maps for the study region from April 2016 until July 2018. Given the fact that temporal changes of albedo in a short timeframe are negligible, the linear interpolation method is expected to result in realistic daily values per pixel (Vanino et al., 2018).

The conditions in Xinavane, with relative humidity ranging between 68 and 75 percent and annual mean daily wind speed below 2 m/s, are favorable to obtain optimal reference evaporation estimates with the Priestley–Taylor equation (Cristea et al., 2012). Therefore, the Priestley–Taylor coefficient can remain 1.26 for the vegetated areas (Priestley and Taylor, 1972; Cristea et al., 2012). For soil pixels, the α value is 1.08 as proposed by Miralles et al. (2011).

2.5. Maximum crop evaporation

The reference evaporation obtained using the Priestley–Taylor equation does not account for the growing stage. Generally, to convert reference evaporation to crop evaporation a crop coefficient (K_c) is used that compensates for the crop type and crop growing stage (Allen et al., 1998). Furthermore, the growing cycle of a crop is divided into three or four crop stages and for each of these crop stages, a different crop coefficient is used. The FAO has provided crop coefficients for each crop stage of some common crops (Allen et al., 1998). The methodology and input used to get from reference evaporation to maximum crop evaporation are visualized in the second column of Fig. 2.

There is a similarity between the evolution of K_c and the Normalized Difference Vegetation Index (NDVI) (Bausch and Neale, 1987). Vegetation absorbs radiation in the visual spectrum and reflects a large amount of infrared radiation. Therefore, a normalized ratio can be used to identify vegetation activity of which the Normalized Difference Vegetation Index (NDVI) has become the most commonly used index today.

NDVI can be translated into a crop coefficient using a simple linear regression model (Kamble et al., 2013). Kamble et al. (2013) showed a strong linear correlation ($r^2=0.91$) between the NDVI and the measured crop coefficients. However, for our study, no measured values are available that can be used for regression. Nonetheless, in this study, the crop factors of ratoon sugarcane that are proposed in Allen et al. (1998) will be used to compensate for the growing stage of the sugarcane.

Mean NDVI data per observation along the growing period was obtained for the fields XNC19, XND18, 20, and XNE18–21, 23. These fields were selected because of their increasing NDVI curve. Next, using the planting and harvest dates of each field, the NDVI data of each crop cycle were obtained. Furthermore, temperature data for each crop cycle was used to convert growing days to Cumulative Growing Degree Days (CGDD), in order to correct for the influence of temperature on the crop development over the growing season (Lofton et al., 2012), see Fig. 3. A quadratic regression resulting from the NDVI observations was used to obtain an NDVI curve as a function of CGDD.

According to Allen et al. (1998) and Doorenbos and Kassam (1979), the initial crop stage has a crop coefficient of 0.4 for ratooned sugarcane and 1.25 when the canopy is at its peak size, and 0.7 at the

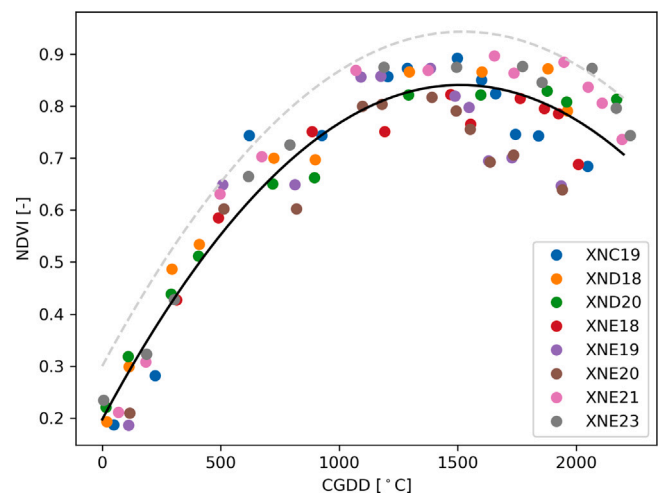


Fig. 3. NDVI observations per field are visualized in relation to CGDD. Fields XNC19, XND18, 20, and XNE18–21, 23 were used to create a crop growth curve. The black line indicates the quadratic regression curve fitting the NDVI observations $NDVI_{est}$. The dotted gray line indicates the optimal NDVI curve $NDVI_{opt}$.

end of the growing season. These crop factors were used as boundaries to translate the $NDVI_{est}$ to a crop coefficient curve dependent on the CGDD:

$$K_c = -6.24 \times 10^{-7} \times CGDD^2 + 1.51 \times 10^{-3} \times CGDD + 0.4 \quad (4)$$

2.6. Actual evaporation

In the last part of the analysis, we tested whether crop stress is visible within NDVI and albedo values in different crop stages to test a methodology to correct maximum crop evaporation estimates for crop stress to retrieve actual evaporation. The methodology and input used in this step are visualized in the third column of Fig. 3. By looking at three performance groups, based on their yield obtained from ground observations (Section 2.3), we assess whether the spectral indices are significantly different from each other in different growth stages. It is assumed that if there is a lot of non-uniformity within a field, then this is related to either mismanagement and/or stress within a field. The non-uniformity should be visible in high spatial resolution spectral indices (Ač et al., 2015).

In order to test if the non-uniformity is present within different crop stages, we first look at the coefficient of variation (CV) of NDVI and albedo within differently performing fields in different crop stages. Then, the statistical significance was tested of the distribution of spectral indices within the different groups. Moreover, the mean value and CV of a field per observation were used as samples for the Mann–Whitney U test. The observations within the groups of fields were at times not normally distributed and the groups showed unequal variances. Therefore the Mann–Whitney U test was found to be most suitable for the analysis (Mann and Whitney, 1947). A significance level of 0.05 was chosen. In each crop stage we tested whether the mean and CV values of NDVI and albedo of the observations within each growth stage were significantly different from each other. In other words, we tested whether the performance groups could be distinguished based on NDVI or albedo.

Ultimately, the relationship between actual NDVI compared to the optimal NDVI was used to account for stress in the evaporation estimate per time step. The optimal NDVI curve, $NDVI_{opt}$, is assumed to be above the estimated NDVI curve as the boundary between sugarcane and bare soil is set where NDVI is 0.3:

$$NDVI_{opt} = -2.78 \times 10^{-7} \times CGDD^2 + 8.46 \times 10^{-4} \times CGDD + 0.3 \quad (5)$$

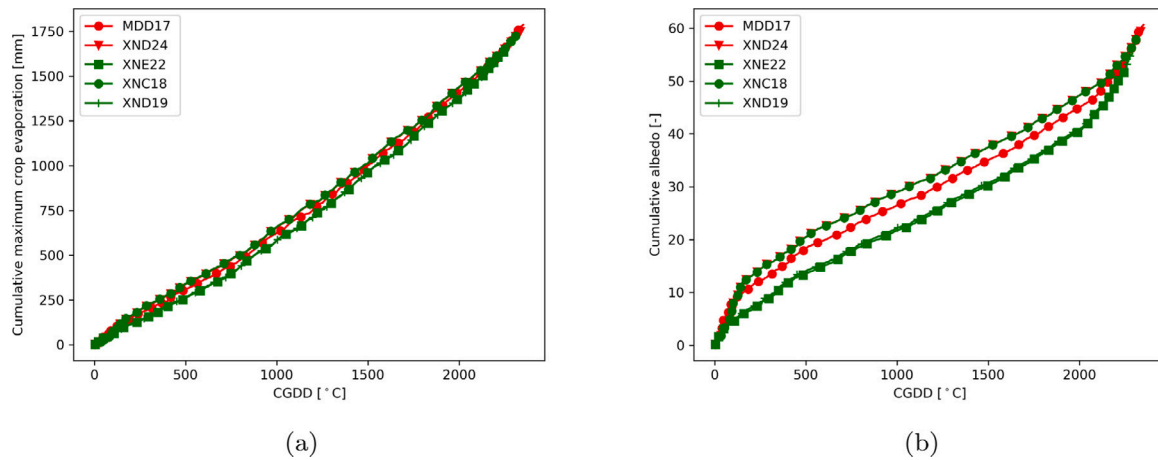


Fig. 4. Figure (a) shows the cumulative maximum crop evaporation in mm for five selected fields (see group 1, Table 1). The red lines indicate the cumulative maximum crop evaporation for fields with a poor yield in seasons 2016/2017. The green lines indicate fields with a medium or good yield. Figure (b) shows the same selected fields, but in this figure the cumulative albedo is displayed against the cumulative growth degree days.

To compute actual evaporation from maximum crop evaporation, the following stress factor was applied:

$$F_s = \begin{cases} \frac{NDVI}{NDVI_{opt}} & \text{for } NDVI \leq NDVI_{opt} \\ 1 & \text{for } NDVI > NDVI_{opt} \end{cases} \quad (6)$$

Where a value of 1 indicates no stress and a value of 0 indicates maximum stress.

3. Results and discussion

3.1. Maximum crop evaporation

In Fig. 4 the evolution of maximum crop evaporation and albedo over CGDD is presented for five selected fields. A similar analysis was done for other groups within the selected 24 fields, but the results do not differ. Within the two figures we zoom in to the difference in maximum crop evaporation and albedo over the growing season.

In theory, the albedo is affected when crop stress is present (Wang and Davidson, 2007). For instance, the albedo of leaves facing water-stress is higher than well-watered leaves (Wang et al., 2004). Therefore, working with high spatial resolution albedo estimates may already include crop stress in the maximum crop evaporation calculations. Fig. 4, however, shows that the difference in albedo between fields is marginal.

A difference between the albedo can only be observed in the first 150 CGDD, this can be explained by the difference in the start date of the growing season (which is determined by the harvesting date of the previous season). The growing season of fields MDD17, XND24, and XNC18 starts earlier than fields XNE22 and XND19 (see Table 1). In Fig. 4b fields MDD17, XND24, and XNC18 therefore show a steeper increase in the first 150 CGDD, which results from a higher albedo in this first part. The albedo increases when sugarcane grows. The sugarcane in fields MDD17, XND24, and XNC18 grow faster at the start. After the difference at the start, the albedo evolution in the different fields have the same shape. Finally, there is barely a difference in cumulative albedo at the end of the season.

The maximum crop evaporation estimates in Fig. 4b also confirm insignificant differences between selected fields. The albedo estimates, therefore, do not include crop stress directly. The reason why crop stress is not directly visible in the albedo estimates results from the methodology applied to retrieve albedo estimates, where MODIS is downscaled with Sentinel-2 bands. The evaporation estimates derived in Fig. 4a, barely include crop stress and can be used to calculate maximum crop evaporation.

3.2. Detecting crop stress

In Fig. 5 we consider the CV of NDVI and albedo within the different performance categories in different growth stages. Similar to the results in Fig. 4, the albedo estimates are not able to distinguish between good and poor performing fields, except for the development stage. The CV values in all growth stages are very low (min=0.003, max=0.0325). This indicates a marginal variability in albedo estimates, resulting from the MODIS correction.

However, considering CV values of NDVI are in Fig. 5, it is possible to distinguish good, medium, and poor performing fields in the development and final stage. The CV of NDVI shows on average a strong negative correlation between the CV and yield in the last two stages.

NDVI is able to distinguish between good and poor performing fields in the last two stages, see Table 3 in the Appendix. The results of the Mann-Whitney U test to distinguish the different groups within crop growth stages shows the different groups can be distinguished based on the NDVI. However, in earlier growth stages the performance categories are not distinguished by the NDVI.

A thick canopy cover, like sugarcane, challenges the performance of spectral indices. Baghdadi et al. (2009) found a similar outcome in the NDVI signal, where NDVI saturated after a height of 150 cm. Saturation effects in spectral indices of sugarcane were also documented by Simões et al. (2009). Only in the case of significant differences, where non- or barely-vegetated pixels are present, spatial heterogeneity is detectable. Such as at the last two stages in Fig. 5 where there is a significant contrast between good and poor performing fields. Molijn et al. (2019) found high spatial resolution NDVI imagery best suitable to monitor sugarcane crop growth compared to different Synthetic Aperture Radar (SAR) products. Molijn et al. (2019) found saturation of NDVI around 80 tonnes/ha. This may explain the results presented in Fig. 5 and Table 3 in the Appendix, where we are able to distinguish between poor and good performing fields based on the CV of NDVI and mean NDVI in the last two growth stages.

Additionally, Molijn et al. (2019) point out the inconsistencies when relating early crop growth imagery with later imagery. The NDVI in the first crop stages shows more variability between images in their analysis. The inconsistencies found by Molijn et al. (2019) in NDVI at the start of the growing period can explain partly the reason why the start of the growing season is not indicative of the biomass production or final yield. This corresponds with the results in Fig. 5.

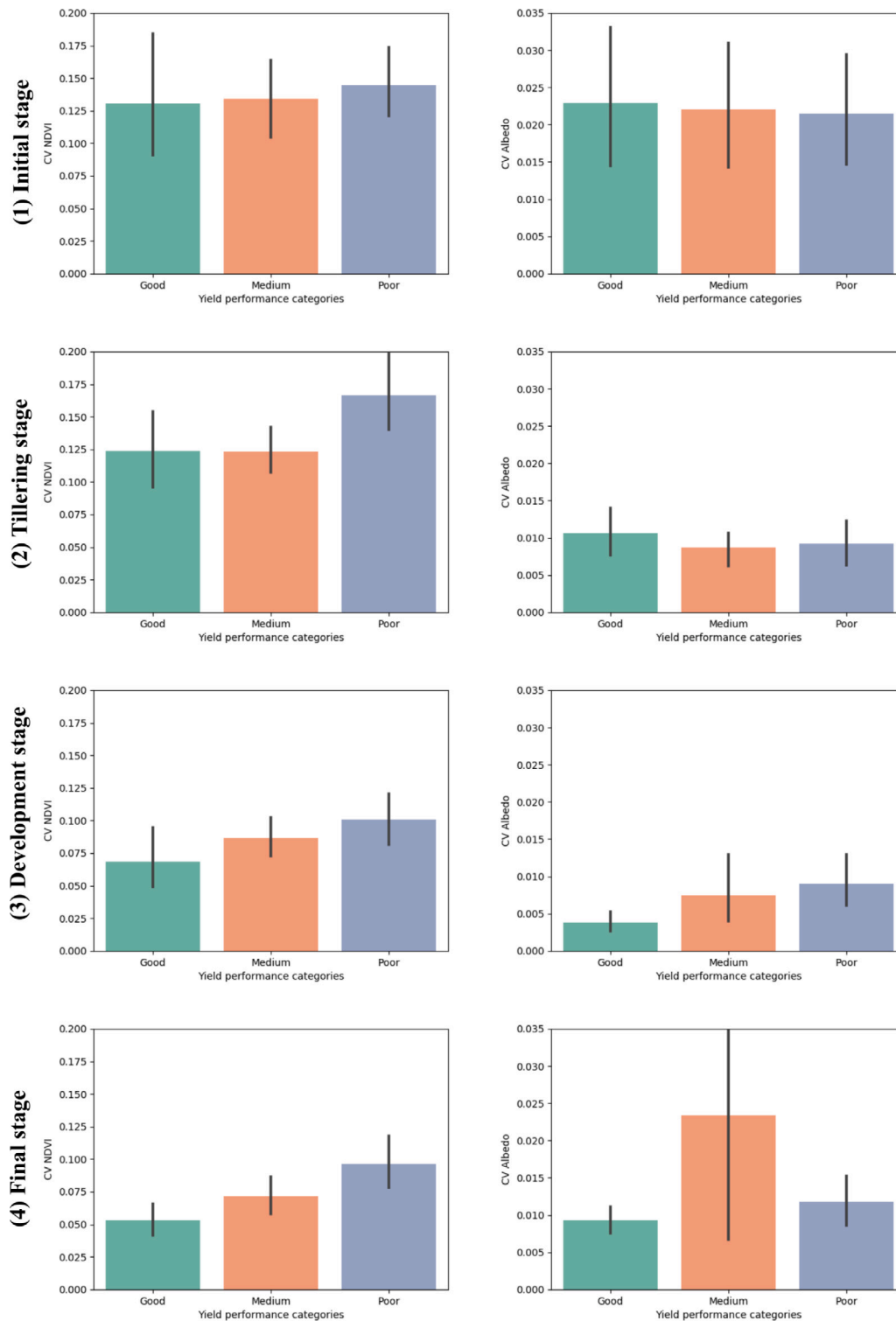


Fig. 5. The first and second column represent the NDVI and Albedo, respectively. The rows present the different growth stages of sugarcane and the relation of NDVI in the different performance categories.

3.3. Actual evaporation

In the fields considered for analysis in group 1, mean actual evaporation per field ranged between 1390 and 1483 mm/season, with minimum values of 693 mm/season and maximum 1589 mm/season. There is a large difference between actual evaporation values within fields. To compare the actual evaporation estimates, we consult another

actual evaporation product with a different methodology (FAO). For the years 2016 and 2017, yearly values between 1098 to 1505 mm/season and 1013 to 1513 mm/season were documented within WAPOR for the same area. These estimates are also in line with the reported industry standard sugarcane ET of 1365 mm/season in the sugarcane states in Swaziland that are located near the Mozambique border (Karimi et al., 2019).

Fig. 6 presents the accumulated difference between maximum crop evaporation and actual evaporation over the growing period within each pixel and field. Each pixel in figure Table 2 indicates accumulated stress. The three fields with a good performance, indicating 110.3, 93.5 and 92.5 tonnes/ha, show a small difference between maximum crop and actual evaporation. In these fields, the mean field difference is 91 mm/season, 93 mm/season, and 126 mm/season respectively. The fields with a yield of 50.4 and 44.0 tonnes/ha indicate a large difference between the maximum crop and actual evaporation. In these fields the mean field difference is 223 mm/season and 335 mm/season respectively. A large difference between maximum crop and actual evaporation indicates more stress.

Additionally, Table 2 shows the effect of harvest date on the difference between maximum crop and actual evaporation. In groups 1 and 3 this difference is smaller than in group 2. Group 2 the difference between maximum crop evaporation and actual evaporation is 259 mm/season or more. The larger difference can be explained by the harvest date. The harvest dates of the fields in groups 1 and 3 lie around June, whereas the harvest dates in group 2 are around the end of November. This is in line with expectation as the yield decreases with harvest dates towards the end of the year. Fields with a harvest date at the end of a calendar year experience nearly two times the rainy season within their growing season. This is the period with the highest evaporation rates and largest difference between maximum crop and actual evaporation.

Using NDVI to incorporate stress in actual evaporation calculations it is possible to distinguish between differently performing fields. NDVI is indicative of the chlorophyll content in the crop or irregularities in sugarcane growth, which can be affected by several factors besides drought. To continue, NDVI can identify hampered growth due to soil nutrition deficits, poor drainage, or secondary salinity effects, amongst other factors. However, to assist irrigation the spatial evaporation estimates need to distinguish between drought-related stress and other crop stresses to prevent overirrigation. This pitfall in current satellite based evaporation algorithms is also identified by Jones (2016). With regard to crop monitoring, the spatial information provided in Fig. 6 can already identify problematic fields and in-field irregularities which can provide valuable information for on-site agronomists.

4. Conclusion

The objective of this study was to determine daily actual evaporation estimates at 20 m resolution for a furrow irrigated site of a large sugarcane plantation in Xinavane, Mozambique, using a combination of satellite imagery and local weather data. A method is set up to apply the Priestley–Taylor methodology spatially and demonstrate the accompanied steps.

Creating a crop growth curve from NDVI as a function of CGDD, allowed the correction of the reference evaporation to the specific growth stage. This resulted in maximum crop evaporation estimates. Identifying stress with spectral indices on a daily scale and with the current resolution of the Sentinel-2 imagery is challenging. Analysis was done to compare the spectral indices of good, medium, and poor performing fields in different growth stages. Albedo estimates show little spatial variability. NDVI in different crop stages in different performance categories showed better results.

With crop yield data and NDVI images per observation from the plantation, different categories of differently performing fields were detected. Especially in the last crop stages the poor, medium, and good performing fields could be distinguished by NDVI observations.

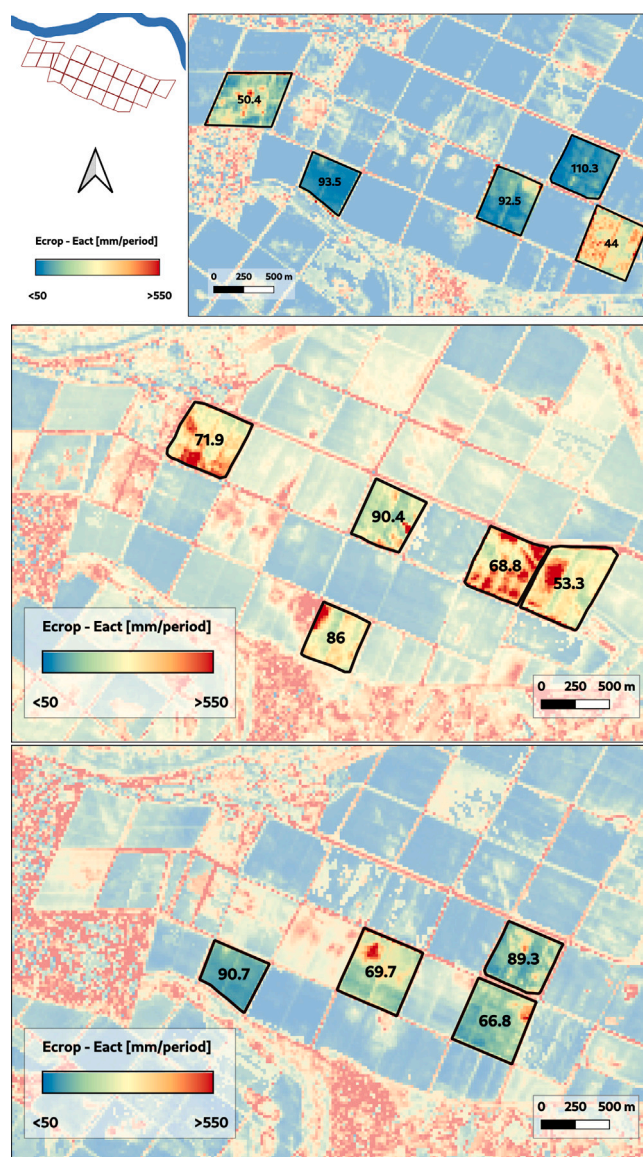


Fig. 6. The difference between maximum crop potential and actual evaporation is presented. Figures A, B, and C zoom in on different groups sugarcane fields with similar growing periods. The fields presented show simulations of the fields with their corresponding plant and harvest dates, as explained in the methodology. The numbers in each field indicate the yield in tonne/ha.

Therefore, NDVI shows potential to be used as an input for a crop stress adjustment factor. This adjustment factor can be used to incorporate crop stress in the maximum crop evaporation calculations to obtain actual evaporation estimates. Testing the consistency of the methodology should be part of future research with a larger database and preferably at different geographic locations. Additionally, the methodology can benefit from a comparison with in situ field measurements.

In practice irrigation scheduling is often based on calculations which considers point-based meteorological data. Spatial visualization of the evaporation fluxes will give farmers and/ or plantations an overview of crop development and growth irregularities. However, in order to be of use to irrigation scheduling, the identified crop stress should be related to drought stress to prevent over-irrigation. The proposed methodology sets a first step in deriving an operational high spatial and temporal resolution of the actual evaporation flux.

Table 2

An overview of three groups of fields that were considered for analysis with a similar harvest date and length of growing season.

Group 1					
	XNC18 (ratoon 5)	XNE22 (ratoon 4)	XND19 (ratoon 8)	XND24 (ratoon 8)	MDD17 (ratoon 7)
Yield 2017 (tonne/ha)	110.3	93.5	92.5	50.4	44.0
Ecrop-Eact: mean (std)	91 ($\sigma=23$)	93 ($\sigma=51$)	126 ($\sigma=63$)	223 ($\sigma=95$)	334 ($\sigma=88$)
Group 2					
	XNC19 (ratoon 6)	XNE19 (ratoon 4)	XNC22 (ratoon 5)	MDC17 (ratoon 7)	MDC16 (ratoon 7)
Yield 2017 (tonne/ha)	90.4	86	71.9	68.8	53.3
Ecrop-Eact: mean (std)	259 ($\sigma=84$)	322 ($\sigma=89$)	361 ($\sigma=93$)	411 ($\sigma=121$)	345 ($\sigma=113$)
Group 3					
	XNE22 (ratoon 5)	XNC18 (ratoon 6)	XND20 (ratoon 9)	XND18 (ratoon 8)	
Yield 2018 (tonne/ha)	90.7	89.3	69.7	66.8	
Ecrop-Eact: mean (std)	129 ($\sigma=39$)	187 ($\sigma=67$)	265 ($\sigma=101$)	193 ($\sigma=77$)	

Table 3

NDVI results. The results in this table present the outcome of the Mann-Whitney U test for mean NDVI in different crop stages.

	Good-Poor	Good-Medium	Medium-Poor
Stage 1	U-Statistic = 353 P-value = 0.27 Sample size — Good: 29 Sample size — Poor: 27	U-Statistic = 151 P-value = 0.16 Sample size — Good: 29 Sample size — Medium: 13	U-Statistic = 159 P-value = 0.32 Sample size — Medium: 13 Sample size — Poor: 27
Stage 2	U-Statistic = 382 P-value = 0.28 Sample size — Good: 30 Sample size — Poor: 28	U-Statistic = 234 P-value = 0.45 Sample size — Good: 30 Sample size — Medium: 16	U-Statistic = 203 P-value = 0.31 Sample size — Medium: 16 Sample size — Poor: 28
Stage 3	U-Statistic = 1073 P-value = 0.02 Sample size — Good: 42 Sample size — Poor: 67	U-Statistic = 503 P-value = 0.16 Sample size — Good: 42 Sample size — Medium: 28	U-Statistic = 831 P-value = 0.2 Sample size — Medium: 28 Sample size — Poor: 67
Stage 4	U-Statistic = 337 P-value = 3.44×10^{-7} Sample size — Good: 41 Sample size — Poor: 44	U-Statistic = 260 P-value = 0.003 Sample size — Good: 41 Sample size — Medium: 22	U-Statistic = 339 P-value = 0.02 Sample size — Medium: 22 Sample size — Poor: 44

Table 4

Albedo results. The results in this table present the outcome of the Mann-Whitney U test for mean albedo in different crop stages.

	Good-Poor	Good-Medium	Medium-Poor
Stage 1	U-Statistic = 382 P-value = 0.44 Sample size — Good: 29 Sample size — Poor: 27	U-Statistic = 169 P-value = 0.3 Sample size — Good: 29 Sample size — Medium: 13	U-Statistic = 151 P-value = 0.24 Sample size — Medium: 13 Sample size — Poor: 27
Stage 2	U-Statistic = 306 P-value = 0.04 Sample size — Good: 30 Sample size — Poor: 28	U-Statistic = 223 P-value = 0.35 Sample size — Good: 30 Sample size — Medium: 16	U-Statistic = 178 P-value = 0.13 Sample size — Medium: 16 Sample size — Poor: 28
Stage 3	U-Statistic = 1050 P-value = 0.01 Sample size — Good: 42 Sample size — Poor: 67	U-Statistic = 417 P-value = 0.02 Sample size — Good: 42 Sample size — Medium: 28	U-Statistic = 928 P-value = 0.47 Sample size — Medium: 28 Sample size — Poor: 67
Stage 4	U-Statistic = 480 P-value = 0.0001 Sample size — Good: 41 Sample size — Poor: 44	U-Statistic = 346 P-value = 0.07 Sample size — Good: 41 Sample size — Medium: 22	U-Statistic = 366 P-value = 0.055 Sample size — Medium: 22 Sample size — Poor: 44

CRedit authorship contribution statement

N.I. den Besten: Conceptualization, Formal analysis, Methodology, Software, Writing. **R.C. Kassing:** Formal analysis, Writing. **E. Muchanga:** Writing. **C. Earnshaw:** Data curation. **R.A.M. de Jeu:** Conceptualization, Supervision, Writing. **P. Karimi:** Writing review & editing. **P. van der Zaag:** Supervision, Writing review & editing.

Declaration of competing interest

The authors declare that they have no known competing financial interests or personal relationships that could have appeared to influence the work reported in this paper.

Acknowledgments

The authors want to thank the staff from the agricultural department at Tongaat Hulett Xinavane. Everybody at the department was very cooperative in providing data and thinking along. Also, we would like to thank Neil Lecler and Alisdair Harris from Tongaat Hulett headquarters in Durban for the support from the start of the project. Additionally, we would like to thank the Netherlands Enterprise Agency for subsidizing the work done in this study. The study was part of a bigger project, named IWACA-Tech (<http://www.iwacatech.com/>).

Appendix

See Tables 3 and 4.

References

- Ač, A., Malenovský, Z., Olejníčková, J., Gallé, A., Rascher, U., Mohammed, G., 2015. Meta-analysis assessing potential of steady-state chlorophyll fluorescence for remote sensing detection of plant water, temperature and nitrogen stress. *Remote Sens. Environ.* 168, 420–436.
- Allen, R.G., Pereira, L.S., Raes, D., Smith, M., et al., 1998. Crop evapotranspiration-guidelines for computing crop water requirements-FAO irrigation and drainage paper 56. *Fao, Rome* 300 (9), D05109.
- Anderson, M.C., Norman, J.M., Mecikalski, J.R., Otkin, J.A., Kustas, W.P., 2007. A climatological study of evapotranspiration and moisture stress across the continental United States based on thermal remote sensing: 1. Model formulation. *J. Geophys. Res.: Atmos.* 112 (D10).
- Apan, A., Held, A., Phinn, S., Markley, J., 2004. Detecting sugarcane 'orange rust' disease using EO-1 Hyperion hyperspectral imagery. *Int. J. Remote Sens.* 25 (2), 489–498.
- Aroca, R., 2012. Plant responses to drought stress. From Morphological to Molecular Features. Springer, Berlin Heidelberg.
- Atzberger, C., 2013. Advances in remote sensing of agriculture: Context description, existing operational monitoring systems and major information needs. *Remote Sens.* 5 (2), 949–981.
- Baghdadi, N., Boyer, N., Todoroff, P., El Hajj, M., Bégué, A., 2009. Potential of SAR sensors TerraSAR-X, ASAR/ENVISAT and PALSAR/ALOS for monitoring sugarcane crops on Reunion Island. *Remote Sens. Environ.* 113 (8), 1724–1738.
- Bastiaanssen, W.G., Menenti, M., Feddes, R., Holtslag, A., 1998. A remote sensing surface energy balance algorithm for land (SEBAL). 1. Formulation. *J. Hydrol.* 212, 198–212.
- Bastiaanssen, W.G., Molden, D.J., Makin, I.W., 2000. Remote sensing for irrigated agriculture: Examples from research and possible applications. *Agric. Water Manag.* 46 (2), 137–155.
- Bausch, W.C., Neale, C.M., 1987. Crop coefficients derived from reflected canopy radiation: A concept. *Trans. ASAE* 30 (3), 703–709.
- Berg, R., Carter, D.L., 1980. Furrow erosion and sediment losses on irrigated cropland. *J. Soil Water Conserv.* 35 (6), 267–270.
- Calera, A., Campos, I., Osann, A., D'Urso, G., Menenti, M., 2017. Remote sensing for crop water management: From ET modelling to services for the end users. *Sensors* 17 (5), 1104.
- Chabot, R., Bouarfa, S., Zimmer, D., Chaumont, C., Duprez, C., 2002. Sugarcane transpiration with shallow water-table: Sap flow measurements and modelling. *Agric. Water Manag.* 54 (1), 17–36.
- Chen, Y., Xia, J., Liang, S., Feng, J., Fisher, J.B., Li, X., Li, X., Liu, S., Ma, Z., Miyata, A., et al., 2014. Comparison of satellite-based evapotranspiration models over terrestrial ecosystems in China. *Remote Sens. Environ.* 140, 279–293.
- Cock, J., 2001. Sugarcane growth and development. *Sugar Cane Int.* 5–15.
- Cristea, N.C., Kampf, S.K., Burges, S.J., 2012. Revised coefficients for Priestley-Taylor and Makkink-Hansen equations for estimating daily reference evapotranspiration. *J. Hydrol. Eng.* 18 (10), 1289–1300.
- Doorenbos, J., Kassam, A., 1979. Yield response to water. *Irrigation Drainage Paper* 33, 257.
- Doorenbos, J., Pruitt, W., 1977. *Crop Water Requirements*, FAO Irrig. Drain. Pap., 24. Food and Agriculture Organization, Rome.
- Endres, L., Moura dos Santos, C., Verissimo de Souza, G., Menossi, M., Marcelino dos Santos, J.C., et al., 2018. Morphological changes recorded in different phenophases of sugarcane plants subjected to water stress in tropical field conditions. *Aust. J. Crop Sci.* 12 (7), 1041.
- FAO, 2018. *WaPOR Database Methodology: Level 1. Remote Sensing for Water Productivity Technical Report: Methodology Series*, FAO, 72, CC BY-NC-SA 3.0 IGO.
- FAO, 2016a. *AQUASTAT Main database*, food and agriculture organization of the united nations (FAO). <http://www.fao.org/nr/water/aquastat/>. Website (Accessed 27 October 2019).
- FAO, 2016b. *AQUASTAT Main database*, food and agriculture organization of the united nations (FAO). <http://www.fao.org/nr/water/aquastat/data/>. Website (Accessed 27 October 2019).
- Ferreira, T.H., Tsunada, M.S., Bassi, D., Araujo, P., Mattiello, L., Guidelli, G.V., Righetto, G.L., Goncalves, V.R., Lakshmanan, P., Menossi, M., 2017. Sugarcane water stress tolerance mechanisms and its implications on developing biotechnology solutions. *Front. Plant Sci.* 8, 1077.
- Fisher, J., Hook, S., Allen, R., Anderson, M., French, A., Hain, C., Hulley, G., Wood, E., 2015. ECOSTRESS: NASA's next-generation mission to measure evapotranspiration from the international space station. In: *AGU Fall Meeting Abstracts*. pp. 4–13.
- Gelcer, E., Fraise, C., Zotarelli, L., Perondi, D., Malia, H., Ecole, C., Migliaccio, K., 2018. A smart irrigation tool to determine the effects of ENSO on water requirements for tomato production in mozambique. *Water* 10 (12), 1820.
- Glaz, B., Morris, D.R., Daroub, S.H., 2004. Sugarcane photosynthesis, transpiration, and stomatal conductance due to flooding and water table. *Crop Sci.* 44 (5), 1633–1641.
- Gunarathna, M., Sakai, K., Nakandakari, T., Momii, K., Onodera, T., Kaneshiro, H., Uehara, H., Wakasugi, K., 2018. Optimized subsurface irrigation system: The future of sugarcane irrigation. *Water* 10 (3), 314.
- Inman-Bamber, N., McGlinchey, M., 2003. Crop coefficients and water-use estimates for sugarcane based on long-term Bowen ratio energy balance measurements. *Field Crops Res.* 83 (2), 125–138.
- Inman-Bamber, N., Smith, D., 2005. Water relations in sugarcane and response to water deficits. *Field Crops Res.* 92 (2–3), 185–202.
- Jelsma, I., Bolding, A., Slingerland, M., 2010. *Smallholder Sugarcane Production Systems in Xinavane, Mozambique: report from the field*. Plant Production Systems, Plant Systems Group, Wageningen University, Wageningen.
- Jones, H., 2016. Opportunities and pitfalls in the use of thermal sensing for monitoring water stress and transpiration. In: *International Symposium on Sensing Plant Water Status-Methods and Applications in Horticultural Science 1197*. pp. 31–44.
- Kamle, B., Kilic, A., Hubbard, K., 2013. Estimating crop coefficients using remote sensing-based vegetation index. *Remote Sens.* 5 (4), 1588–1602.
- Karimi, P., Bongani, B., Blatchford, M., de Fraiture, C., 2019. Global satellite-based ET products for the local level irrigation management: An application of irrigation performance assessment in the sugarbelt of swaziland. *Remote Sens.* 11 (6), 705.
- Lofton, J., Tubana, B.S., Kanke, Y., Teboh, J., Viator, H., Dalen, M., 2012. Estimating sugarcane yield potential using an in-season determination of normalized difference vegetative index. *Sensors* 12 (6), 7529–7547.
- Louis, J., Debaecker, V., Pflug, B., Main-Knorn, M., Bieniarz, J., Mueller-Wilm, U., Cadau, E., Gascon, F., 2016. Sentinel-2 sen2cor: L2a processor for users. In: *Proceedings of the Living Planet Symposium, Prague, Czech Republic*. pp. 9–13.
- Mann, H.B., Whitney, D.R., 1947. On a test of whether one of two random variables is stochastically larger than the other. *Ann. Math. Stat.* 50–60.
- Martins, M.T.B., de Souza, W.R., da Cunha, B.A.D.B., Basso, M.F., de Oliveira, N.G., Vinecky, F., Martins, P.K., de Oliveira, P.A., Arenque-Musa, B.C., de Souza, A.P., et al., 2016. Characterization of sugarcane (*Saccharum spp.*) leaf senescence: Implications for biofuel production. *Biotechnol. Biofuels* 9 (1), 153.
- Meerdink, S., Hook, S., Abbott, E., Roberts, D., 2018. The ECOSTRESS spectral library 1.0, accessed online, vol. 1, no. 03. <https://speclib.jpl.nasa.gov/library>. Website accessed on (Accessed 1 September 2018).
- Miralles, D., Holmes, T., De Jeu, R., Gash, J., Meesters, A., Dolman, A., et al., 2011. Global land-surface evaporation estimated from satellite-based observations. *Hydrol. Earth Syst. Sci.* 453–469.
- Molijn, R.A., Iannini, L., Vieira Rocha, J., Hanssen, R.F., 2019. Sugarcane productivity mapping through C-Band and L-Band SAR and optical satellite imagery. *Remote Sens.* 11 (9), 1109.
- Mulla, D.J., 2013. Twenty five years of remote sensing in precision agriculture: Key advances and remaining knowledge gaps. *Biosyst. Eng.* 114 (4), 358–371.
- Norman, J.M., Kustas, W.P., Humes, K.S., 1995. Source approach for estimating soil and vegetation energy fluxes in observations of directional radiometric surface temperature. *Agric. Forest Meteorol.* 77 (3–4), 263–293.
- Olivier, F.C., Singels, A., 2015. Increasing water use efficiency of irrigated sugarcane production in South Africa through better agronomic practices. *Field Crops Res.* 176, 87–98.

- Plaut, Z., Meinzer, F.C., Federman, E., 2000. Leaf development, transpiration and ion uptake and distribution in sugarcane cultivars grown under salinity. *Plant Soil* 218 (1–2), 59–69.
- Price, J.C., 1982. Estimation of regional scale evapotranspiration through analysis of satellite thermal-infrared data. *IEEE Trans. Geosci. Remote Sens.* (3), 286–292.
- Priestley, C.H.B., Taylor, R., 1972. On the assessment of surface heat flux and evaporation using large-scale parameters. *Monthly Weather Rev.* 100 (2), 81–92.
- Raine, S., Bakker, D., 1996. Increased furrow irrigation efficiency through better design and management of cane fields. In: *Proceedings-Australian Society of Sugar Cane Technologists*. Watson Ferguson and Company, pp. 119–124.
- Santillán-Fernández, A., Santoyo-Cortés, V., García-Chávez, L., Covarrubias-Gutiérrez, I., Merino, A., 2016. Influence of drought and irrigation on sugarcane yields in different agroecoregions in Mexico. *Agric. Syst.* 143, 126–135.
- Schaaf, C., Wang, Z., 2015. Mcd43D60 MODIS/Terra+Aqua BRDF/Albedo white sky albedo NIR daily l3 global 30arcsec CMG v006 NASA EOSDIS l. process. DAAC. <https://doi.org/10.5067/MODIS/MCD43D60.006>. Website accessed on (accessed 17 April 2019).
- Silva, V., Garcéz, S., Silva, B.d., Albuquerque, M.d., Almeida, R., 2015. Métodos de estimativa da evapotranspiração da cultura da cana-de-açúcar em condições de sequeiro. *Revista Brasileira de Engenharia Agrícola e Ambiental* 19 (5), 411–417.
- Simões, M.d.S., Rocha, J.V., Lamparelli, R.A.C., 2009. Orbital spectral variables, growth analysis and sugarcane yield. *Scientia Agrícola* 66 (4), 451–461.
- Singels, A., Kennedy, A., Bezuidenhout, C., 1998. IRRICANE: A simple computerised irrigation scheduling method for sugarcane. In: *Proc. S. Afr. Sug. Technol. Ass.* vol. 72. pp. 117–122.
- Singh, A., Kumari, V.V., Gupta, R., Singh, P., Solomon, S., 2018. Efficient irrigation water management in sugarcane through alteration of field application parameters under subtropical India. *Sugar Tech.* 20 (1), 21–28.
- Vanino, S., Nino, P., De Michele, C., Bolognesi, S.F., D'Urso, G., Di Bene, C., Pennelli, B., Vuolo, F., Farina, R., Pulighe, G., et al., 2018. Capability of sentinel-2 data for estimating maximum evapotranspiration and irrigation requirements for tomato crop in central Italy. *Remote Sens. Environ.* 215, 452–470.
- Vanino, S., Nino, P., De Michele, C., Bolognesi, S.F., Pulighe, G., 2015. Earth observation for improving irrigation water management: A case-study from Apulia region in Italy. *Agric. Agric. Sci. Procedia* 4, 99–107.
- Viswanadham, Y., Silva Filho, V., Andre, R., 1991. The Priestley-Taylor parameter α for the Amazon forest. *Forest Ecol. Manag.* 38 (3–4), 211–225.
- Vuolo, F., D'Urso, G., De Michele, C., Bianchi, B., Cutting, M., 2015. Satellite-based irrigation advisory services: A common tool for different experiences from Europe to Australia. *Agric. Water Manag.* 147, 82–95.
- Wan, Z., Hook, S., Hulley, G., 2015. Mod11a1 MODIS/Terra land surface temperature/emissivity daily L3 global 1km SIN grid V006. <https://doi.org/10.5067/MODIS/MOD11A1.006>. Website accessed on (Accessed 9 September 2018).
- Wang, S., Davidson, A., 2007. Impact of climate variations on surface albedo of a temperate grassland. *Agricult. Forest Meteorol.* 142 (2–4), 133–142.
- Wang, S., Davidson, A., Latifovic, R., 2004. Impact of drought on land surface albedo. In: *AGU Spring Meeting Abstracts*. p. 85.
- Yadav, R., Shukla, S., Suman, A., Singh, P., 2009. Trichoderma inoculation and trash management effects on soil microbial biomass, soil respiration, nutrient uptake and yield of ratoon sugarcane under subtropical conditions. *Biol. Fertil. Soils* 45 (5), 461–468.
- Van der Zaag, P., Carmo Vaz, Á., 2003. Sharing the incommensurate waters: Cooperation and competition in the balance. *Water Policy* 5 (4), 349–368.